

Single SiV⁻ centers in low-strain nanodiamonds with bulk-like spectral properties and nano-manipulation capabilities

Lachlan J Rogers ^{*,1,2} Ou Wang ^{*,3,4} Yan Liu,³ Lukas Antoniuk,³ Christian Osterkamp,^{3,4,5} Valery A. Davydov,⁶ Viatcheslav N. Agafonov,⁷ Andrea B. Filipovski,³ Fedor Jelezko,^{3,4} and Alexander Kubanek^{3,4}

¹*Department of Physics and Astronomy, Macquarie University, New South Wales 2109, Australia*

²*ARC Centre of Excellence for Engineered Quantum Systems,
Macquarie University, New South Wales 2109, Australia*

³*Institute for Quantum Optics, University Ulm, Albert-Einstein-Allee 11, D-89081 Ulm, Germany*

⁴*Center for Integrated Quantum Science and Technology (IQST),
University Ulm, Albert-Einstein-Allee 11, D-89081 Ulm, Germany*

⁵*Department of Electron Devices and Circuits, University Ulm, Albert Einstein Allee 45, 89069 Ulm, Germany*

⁶*L.F.Vereshchagin Institute for High Pressure Physics,*

Russian Academy of Sciences, Troitsk, Moscow, 142190, Russia

⁷*GREMAN, UMR CNRS CEA 6157, Universit F. Rabelais, F-37200 Tours, France*

The controlled interfacing of individually well-isolated atoms is one of the outstanding challenges for bottom-up assemblies of complex quantum systems. Here, we establish SiV⁻ centers in nanodiamonds as a new potential building block for solid-state based quantum technology. Utilizing an atomic force microscope cantilever we demonstrate controlled nano-manipulation including dipole rotation and cluster decomposition, as well as 1D- and 2D-alignment with ≈ 10 nm accuracy. We employ H-plasma treatment in combination with resonant and off-resonant excitation to isolate single SiV⁻ centers per nanodiamond with improved inhomogeneous ensemble linewidth and stable optical transitions. Our methods allow us to observe fine-structure and to elaborate analytical strain model where we experimentally extract the ratio between strain coefficients of excited and ground states. The observed strain values are as low as best values in low-strain bulk diamond. Together with good polarization contrast and excellent spectral stability under resonant excitation our work paves the way for indistinguishable photon emission and should facilitate the development of new complex quantum systems.

INTRODUCTION

Experimental quantum optics has gradually shifted focus from testing fundamentals of quantum mechanics using isolated quantum systems such as atoms or photons [1, 2] towards the development of quantum technologies utilizing many connected quantum systems. Applications include quantum computation (ion-traps and superconducting technology have achieved several quantum bits [3, 4]) and low entropy systems, realized in atom-by-atom assemblies of up to 100 atoms in one-dimensional defect-free arrays [5]. The central challenge is to balance the need for quantum systems to be well isolated from their environment with the competing requirement that they interact with each other via well-controlled coupling. Coupling mechanisms include magnetic interaction, dipole-dipole interaction, and long-range interaction between distant atoms mediated via photons as employed in photonic quantum technologies [6] or distributed quantum networks [7, 8]. Efficient interfacing requires precise positioning on the relevant scale of the specific coupling mechanism, which is smaller than the electromagnetic field wavelength for optical coupling.

Semiconductor quantum optics is particularly well suited for constructing scalable devices satisfying this requirement, and the silicon-vacancy (SiV⁻) color centre in diamond has emerged as an excellent optical-spin candidate. Single SiV⁻ centers have been coupled to all-diamond photonic platforms [9, 10] and are good sources

of indistinguishable photons [11, 12] with lifetime-limited spectral linewidth, low spectral diffusion in low-strain diamond hosts [13], and a high Debye-Waller factor [14]. Arrays of bright SiV⁻ centers have been created via ion implantation with a yield of up to 15 percent [15]. However a bottom-up approach utilizing single SiV⁻ centers in preselected nanodiamonds (NDs) could enable deterministic emitter assemblies with fault-tolerance via post-processing. This offers a wide-ranging flexibility for hybrid photonic platforms [16–18]. Despite progress with SiV⁻ centers in NDs demonstrating nearly-lifetime limited linewidth [19], they still suffer from surface effects and from a highly strained diamond host with broad inhomogeneous linewidth, large spectral instability and, furthermore, no deterministic way to obtain single NDs containing single SiV⁻ centers.

Here we show that surface treatment of NDs can be used to correct these deficiencies of SiV⁻ optical properties, and furthermore demonstrate nanomanipulation abilities necessary to construct arrays of SiV⁻ emitters for hybrid photonic platforms. An atomic-force microscope probe is used to position NDs in one- and two-dimensional arrays with an accuracy below the uncertainties of the emitter localization of typically ≈ 25 nm limited by the extend of the ND and the lateral resolution of the AFM. In addition, we demonstrate rotation of the NDs for dipole alignment, and decomposition of ND clusters. The toolbox is further expanded by the ability to pick and place individual NDs [16, 18, 20]. We show that

SiV⁻ centers contained in NDs have improved optical properties after surface treatment in hydrogen plasma, and demonstrate for the first time that ND SiV⁻ centers are capable of providing atom-like spectral properties as in bulk diamond. Single SiV⁻ centers are isolated in NDs and their optical transition fine-structure is used to explore the strain of their host crystal environments, with 70% of the SiV⁻ centers exhibiting transversal strain splitting similar to the lowest strain bulk diamond. The natural distribution of strain in the NDs provides the first systematic inference of the SiV⁻ zero-strain orbital splitting, and also the ratio of transverse strain splitting coefficients between ground and excited states. Low-strain SiV⁻ in NDs are shown to exhibit a high degree of optical polarization contrast, almost Fourier-limited linewidth, and spectral stability within the Fourier-limited linewidth over ten minutes. The ability to control and nanomanipulate single SiV⁻ center in NDs with sizes of a few tens of nm and large spectral homogeneity opens new possibilities to optically couple arrays of SiV centers in NDs, exploring novel routes for hybrid quantum technology in fields like quantum networks, quantum sensing, and quantum simulations.

RESULTS

Manipulating NDs on the nanoscale

Positioning NDs containing negatively charged Nitrogen-Vacancy (NV⁻) centers in close proximity to plasmonic structures and within the electromagnetic field mode of a photonic crystal cavity has previously been demonstrated using an atomic force microscope (AFM) [16, 18, 20]. In these studies the positioning precision was determined from the coupling strength to the photonic structure under investigation. Here we performed position manipulation of NDs on the nanoscale using an AFM in high-resolution contact mode. Small NDs with an average diameter of 25 nm were chosen since the diamond size fundamentally limits the uncertainty of localizing the emitter in a confocal microscope. The NDs were preselected to contain NV⁻ centers, since these provide a well-established way to spectrally determine alignment angles to an external magnetic field [21]. The NV⁻ centers were imaged using an integrated confocal fluorescence microscope.

A string of four NDs was aligned and equally spaced with 1.5 μm separation as shown in Figure 1a. The confocal fluorescence images show that bright NDs were moved into a straight line configuration. The AFM lateral resolution is limited by the cantilever tip radius of curvature (nominally $\approx 10\text{ nm}$), and was capable of image spots about 75 nm wide (FWHM). This is considerably better than the diffraction-limited confocal microscope resolution. The final position coordinates of the NDs were obtained from the center of the two-dimensional Gaussian fits to the AFM topographic data. The typical devia-

tion of the ND positions from the target coordinates was found to be $\Delta x_{nn} = 37\text{ nm}$ and $\Delta y_{nn} = 22\text{ nm}$.

On our device, the pushing operation required a “field of view” that included the reference position as well as the desired position. Measurement of separation distance is less precise for a wider-field scan, and so the ND positioning accuracy diminishes with increasing separation from the reference location. ND separations much larger than the optical wavelength were chosen here to extract an lower bound on the positioning accuracy.

Two-dimensional arrays of NDs are more challenging to align, but of great interest for many applications. This capability was demonstrated by arranging a different set of four NDs into a square pattern with separation of 1 μm as shown in Figure 1b. The position deviation from the target coordinates was similar to that observed for the straight-line arrangement, but increased slightly for the corner diagonally opposite the reference ND due to accumulation of successive positioning procedures. All positioning operations were performed with a precision in the order of the ND size, and further precision may be obtained by iterating the procedure with feedback from intermediate measurements of the ND location (see methods for details). The location of the NV⁻ or SiV⁻ emitter within a ND is difficult to obtain, and this represents a fundamental limit on the positioning accuracy of the emitter. We estimate the overall position uncertainty of the emitter is $\approx 40\text{ nm}$, where the size of the ND is the dominant contributing factor.

Optically-detected magnetic resonance (ODMR) was measured for a single NV⁻ center in one ND, and this measurement yields information about the alignment of the NV⁻ center relative to a stationary external magnetic field from a 3-mm-sized magnet cube, which is sitting about 8 mm away from the NDs. The magnet creates a field of $39 \pm 4\text{ Gauss}$ at the measured ND. The observed resonance frequencies of $2834.8 \pm 0.1\text{ MHz}$ and $2913.8 \pm 0.2\text{ MHz}$ (Figure 1c, uncertainties deduced from Lorentz fitting) correspond to an angle of $69 \pm 2^\circ$ between the NV⁻ symmetry axis and the magnetic field. This ND was moved approximately 100 nm, and the ODMR resonance frequencies changed to $2788.3 \pm 0.1\text{ MHz}$ and $2954.0 \pm 0.1\text{ MHz}$, corresponding to an angle of a $38 \pm 6^\circ$ relative to the external field. It is concluded that the manipulation rotated the ND by approximately $31 \pm 5^\circ$, which is the first demonstration of a potential dipole alignment procedure by rotational ND manipulation. The calculation of magnetic field as well as the angle between NV⁻ symmetry axis and the magnetic field using ODMR frequencies of NV⁻ was done according to Ref. [21]. The comparatively large uncertainties in angle arise mainly from the fact that the zero-field splitting is only known to a precision of $\pm 1\text{ MHz}$ [22] at room temperature. For more precise final alignment, an order of magnitude improvement would be possible if the zero field splitting was measured for the specific NV⁻ centre under investigation (see method section for details).

NDs commonly form clusters when they are dispersed

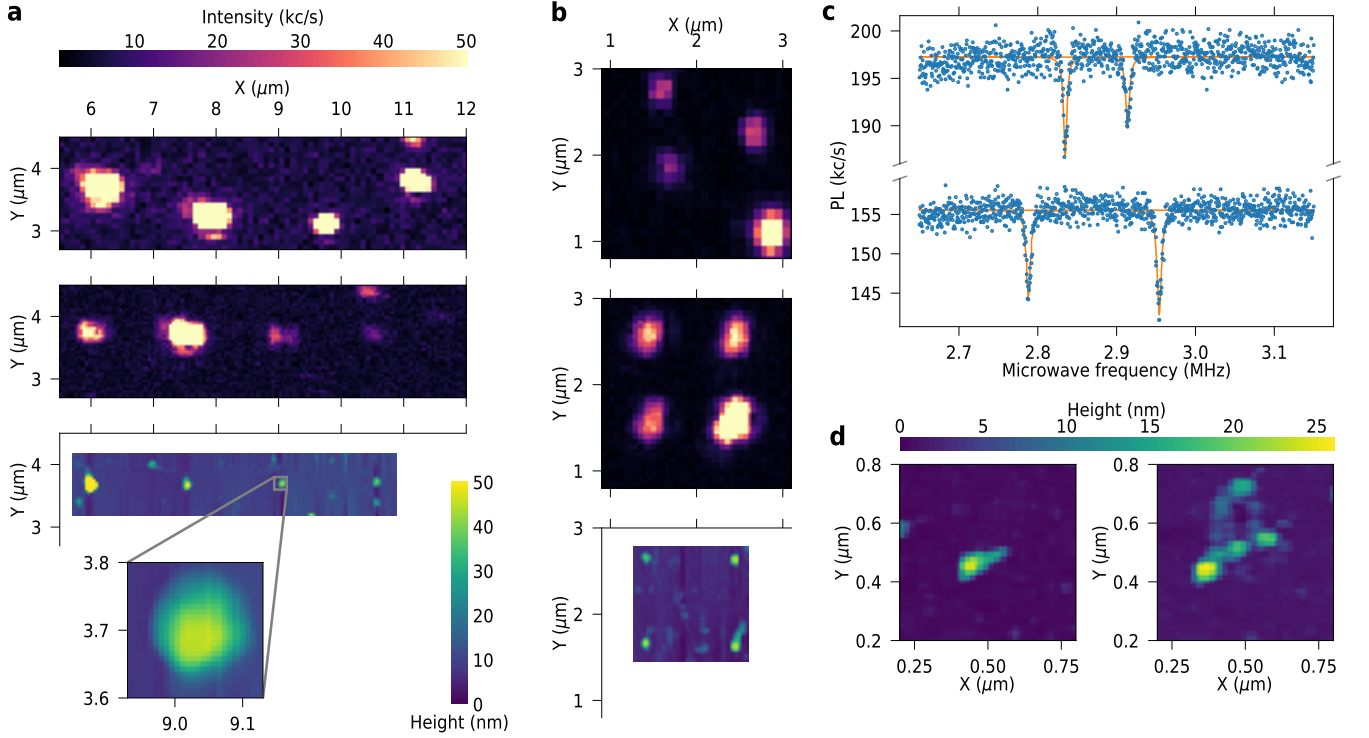


FIG. 1. Manipulation of NDs at nanoscale: **a** 1D alignment of 4 NDs with an accuracy of 37 nm. From top to bottom: Fluorescence image of spin-coated ND sample on glass; fluorescence image of the same sample area after nanos positioning procedure with the AFM in contact mode; topography image of the aligned 4-ND string with the AC-mode of the AFM. The inset shows the AFM resolution, which has a full-width at half-maximum of 75 nm. **b** 2D nanos positioning with accuracy of 37 nm. From top to bottom: Fluorescence image of spin-coated ND sample on glass; fluorescence image after nanos positioning procedure of AFM with contact mode; topography image of the aligned 4-ND square with AC-mode of AFM. The colour bars are shared with part **a**. **c** Demonstration of NV axis rotation during one tip-push with the AFM in contact mode with pushing distance ~ 100 nm in a constant magnetic field. Before the rotation (above) the resonant frequencies are 2834.8 ± 0.1 MHz and 2913.8 ± 0.2 MHz, corresponding to 39 ± 4 Gauss and the angle between NV axis and magnetic field $\theta = 69 \pm 2^\circ$. After the rotation (below) the resonant frequencies are 2788.3 ± 0.1 MHz and 2954.0 ± 0.1 MHz, corresponding to 38 ± 4 Gauss and corresponding to $\theta = 38 \pm 6^\circ$. **d** Decomposition of a ND cluster. Larger clusters of ND (left image) can be decomposed by pressing the AFM cantilever into the cluster (right image).

on a substrate, and various techniques have been developed to discourage this phenomenon. Figure 1d shows an AFM topographical scan of a ND cluster before and after the cantilever was pushed into contact. It is apparent that manipulation with the AFM tip is capable of decomposing a ND cluster into its individual components.

Surface treatment of NDs to alter SiV^- optical properties

Intrinsic SiV^- centers form during growth of NDs synthesized under chemical vapor deposition [23] and also under direct high-pressure high-temperature (HPHT) synthesis [24]. HPHT conditions effectively allow crystal annealing during growth, which can lead to the production of low-strain NDs. HPHT NDs have previously been found to host SiV^- centers with excellent optical properties [19], and these same ND samples were used here. The NDs were size-selected using a centrifuge (procedure

outlined in the methods section) and were spin-coated on H^{a} diamond substrates containing markers produced by selective carbon milling [19]. The typical ND size was around or below 130 nm, and physical dimensions of specific NDs under study were obtained by SEM imaging that was spatially correlated with fluorescence images using the substrate markers.

Previous spectroscopic investigations of SiV^- centres in these HPHT NDs suggested that the optical properties were impacted and in some ways limited by effects on the ND surface [19]. In particular, the photoluminescence (PL) spectrum of the zero-phonon lines of SiV^- centres exhibit undesired spectral diffusion. This was characterized with off-resonant excitation at 532 nm and at cryogenic temperatures of 8 K (apparatus described in Methods), where groups of narrow lines around 737 nm were observed in photoluminescence (PL) as shown in shown in Figure 2a. These features in the spectrum arise from the direct optical transitions of SiV^- centres, and it is apparent that they shift position and sometimes

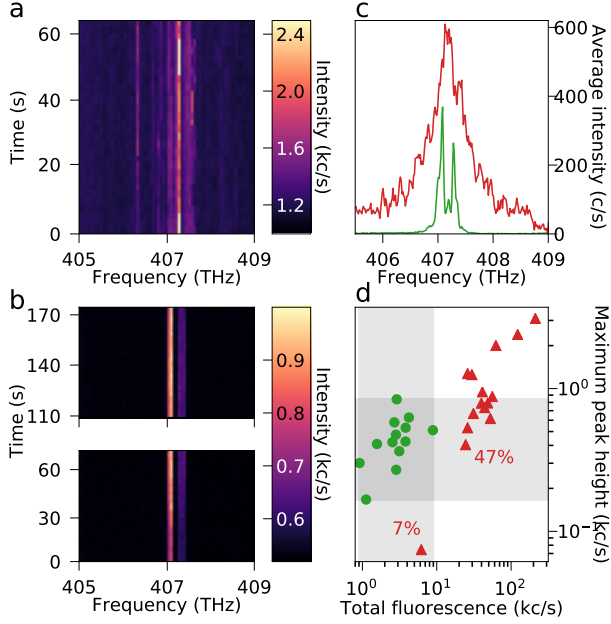


FIG. 2. Comparison of optical properties between untreated and H-plasma treated SiV^- in NDs at cryogenic temperature. **a** Time-resolved spectra of SiV^- in untreated ND sample with multiple lines and spectral diffusion. **b** Time-resolved spectra of SiV^- in H-plasma treated ND sample, which presents the 4-line fine structure of SiV^- ZPL, with no spectrometer-resolvable spectral diffusion. The discontinuity of time between 70 s – 110 s was due to the refocusing with confocal microscope. **c** The broader red peak shows the inhomogeneous spectrum from untreated ND sample. The narrower green spectrum, where doublet-like fine-structures can be resolved, shows the inhomogeneous spectrum of spectrally-stable points from H-plasma treated ND sample. **d** Scattered plots comparing the total fluorescence and maximum peak height of POIs H-plasma treated (green dots) and untreated (red triangles) sample. As illustrated by the blue shadow, while 47 % of the points from the untreated sample have a maximum peak height that lies in the same range as the H-plasma treated sample, there is only 7 % of spots from the untreated sample emitting a total fluorescence that lies in the same range as the H-plasma treated ones.

blink over the measurement duration. Taking the time-averaged emission from these measurement and summing across 15 different spots produced the small-ensemble PL spectrum shown in red in Figure 2c. The characteristic four-line pattern of the SiV^- zero-phonon line [13, 25] cannot be resolved, indicating that the inhomogeneous spread of SiV^- centers in this ensemble is broader than the 252 GHz excited state splitting. This result is consistent with previous reports [19], and is a fundamental limitation to many applications when continuous resonant excitation of individual optical transition is required.

A part of this ND sample was treated in a hydrogen plasma (see methods), and time-resolved PL spectra were measured for 23 spots containing SiV^- . The PL spectra of SiV^- transitions in the treated NDs showed signifi-

cantly improved spectral stability, and a typical measurement is shown in Figure 2b. In addition, the four line fine-structure of SiV^- was clearly visible in the PL spectrum for 17 of the 23 points investigated (see supplementary information). For two points we observed broader spectral peaks in a stable doublet, which may be attributed to a thermal broadening of the peaks with higher temperatures due to small contacting area between those NDs and the substrate. The small-ensemble spectrum (green curve in Figure 2c) integrated for the stable spectra in the treated sample clearly has a doublet structure, indicating that the inhomogeneous distribution is narrower than the 252 GHz excited state splitting.

We compare the PL spectra from the treated sample with the PL spectra from the untreated sample at cryogenic temperature and with identical experimental setting. As shown in Figure 2d, there was only a minor effect on the maximum peak height by H-termination, as 47 % of the untreated points from the untreated sample lies in the same range as H-plasma treated ones. In contrast, the total fluorescence altered significantly (within the range between 733 nm to 741 nm) with an overlap quantity of only 7 %. This indicates that the surface treatment reduces the brightness of the NDs by “switching off” some of the SiV^- centers, but that the remaining ones are just as bright as they were before treatment. If more than one emitter is present in a focal spot overlapping emission lines could lead to a change in maximum peak height in a spectrum. However, the large inhomogeneous spectral distribution in the untreated NDs suggests a small likelihood of overlapping emission lines between SiV^- centers in any given ND. In addition, SiV^- centers in untreated NDs gave a $g^2(\tau)$ auto-correlation function with no visible dip at $\tau = 0$ (the signature of single quantum emitters) whereas SiV^- fluorescence from the treated NDs showed clear sub-Poissonian emission with $g^2(0)$ down to 0.2 after background correction (see supplementary information). This strengthens the interpretation that the surface treatment has reduced the number of active SiV^- centers in the NDs, and indicates the possibility to isolate single, most stable SiV^- center per ND even under off-resonant excitation.

Strain analysis of the fine-structure of SiV^- in NDs

Variation in the ZPL lines between NDs is attributed primarily to differences in strain. The 2E_g ground and 2E_u excited states each have twofold orbital degeneracy, and are intrinsically split by spin-orbit interaction as illustrated in Figure 3a [25]. Strain aligned with the symmetry axis of the SiV^- centre does not lower the symmetry and so cannot lift the orbital degeneracy, but it can shift the energies of the ground and excited states and this appears as a shift in the position of the ZPL. Strain transverse to the symmetry axis does lift the orbital degeneracy, splitting the E_x and E_y orbitals apart in energy. This is observed as an increase in the splitting

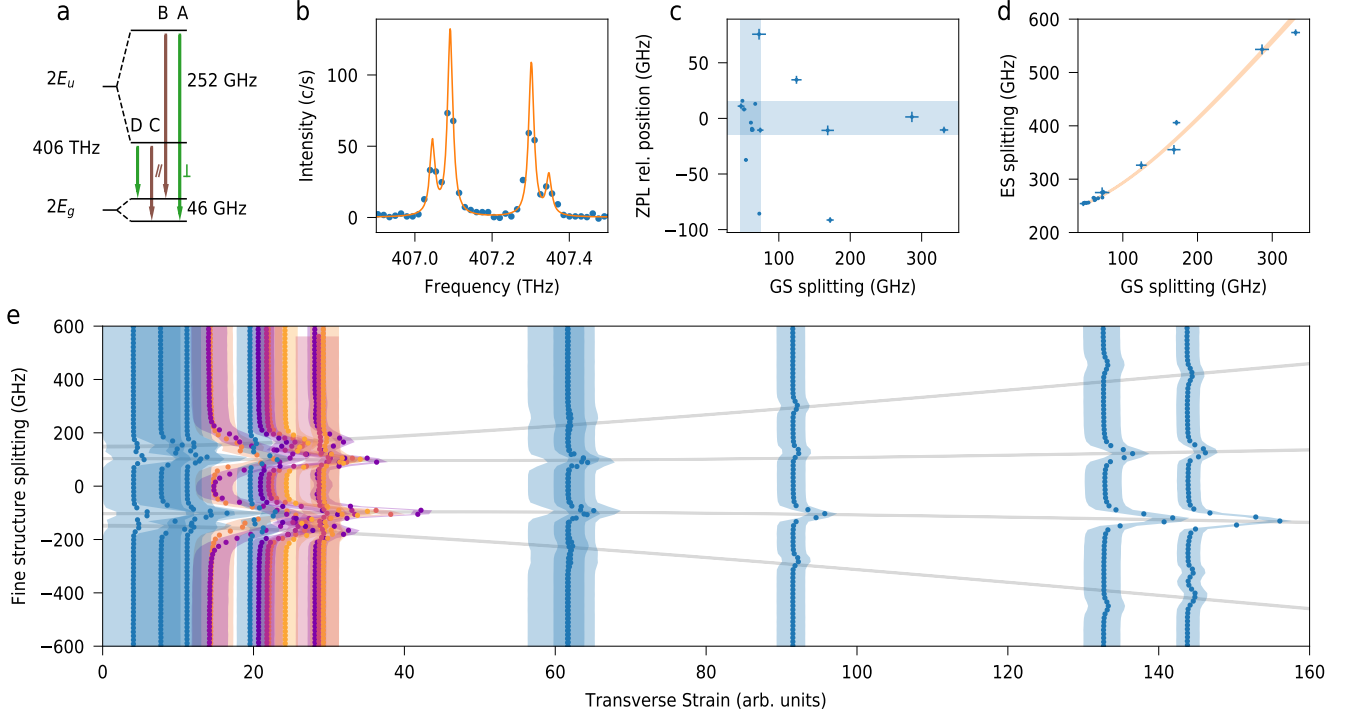


FIG. 3. Strain analysis of SiV^- centres in the nanodiamond environment. **a** The SiV^- electronic structure has orbitally-degenerate ground and excited states with intrinsic splitting resulting from spin-orbit interaction. Optical transitions A and D are polarized perpendicular to the SiV^- symmetry axis while B and C are parallel. **b** The four optical transitions are resolved at low temperature in the PL spectrum. Axial (transverse) strain alters the position (splitting) of these spectral lines. **c** The four-line PL spectrum was clearly identified in 17 of the 23 spots measured, and the splittings determined. There is no correlation between the SiV^- ground state splitting and the ZPL central frequency, due to the random orientation of strain in the NDs. The 30×30 GHz shaded region is interpreted as low strain and contains 8 out of the 17 NDs. **d** The transverse strain component can be isolated by considering only the splittings, and there is close correlation between ground state splitting and excited state splitting. These data indicate that the excited state strain splitting coefficient is $1.688^{+0.008}_{-0.008}$ times larger than that of the ground state. **e** Statistical inference of the SiV^- strain splitting from 18 PL spectra (a spot with unresolved four line pattern was suitable for this analysis). The grey lines shade the 95% credible region for the optical transition energies split by transverse strain, and provide the first systematic identification of the SiV^- zero-field splittings in the ground ($46.3^{+2.5}_{-3.4}$ GHz) and excited ($252.0^{+1.3}_{-1.8}$ GHz) states. Each spectrum is placed at its inferred transverse strain value, with the shaded band corresponding to the 95% credible region. The spectra between 14 and 30 strain units are coloured to aid visual differentiation. Thirteen of the SiV^- spectra correspond to the low-transverse-strain situation where the splitting is dominated by spin-orbit interaction (increasing the chances of spectrally identical emitters).

between fine-structure peaks in the ZPL, which are resolved in cryogenic PL as shown in Figure 3b. The ZPL position and the splittings for ground and excited states were determined for each SiV^- that showed a clear four-line spectrum. Figure 3c shows the position versus the ground state splitting, which essentially corresponds to axial strain versus transverse strain. There is no correlation, which is consistent with a random orientation of the strain in the NDs relative to the SiV^- symmetry axis. This comparison is further complicated by the numerous unrelated effects such as temperature [26] and isotopic shift [27] which can shift the SiV^- transitions (but not cause splitting). It is however apparent that almost half of the SiV^- spectra are clustered fairly close together near the minimum ground-state splitting, shaded in Figure 3c.

Spectral splitting indicates splitting of the orbital degeneracy in the E ground and excited states. Unlike the line position, transverse strain is the most likely cause of orbital splitting and so the spectral splitting can provide more information about strain. Figure 3d shows the excited-state splitting versus the ground-state splitting, and a strong correlation is apparent. This is expected for transverse strain, which must be the same for ground and excited states of a localized SiV^- center. Transverse strain was modelled for the four-level system illustrated in Figure 3a using the standard strain Hamiltonian

$$\begin{bmatrix} \nu + \frac{1}{2}\lambda_{\text{SO}}^e & \delta E^e & & \\ \delta E^e & \nu - \frac{1}{2}\lambda_{\text{SO}}^e & & \\ & & \frac{1}{2}\lambda_{\text{SO}}^g & \delta E^g \\ & & \delta E^g & \frac{1}{2}\lambda_{\text{SO}}^g \end{bmatrix} \quad (1)$$

where ν is the optical transition frequency, λ_{SO}^e and λ_{SO}^g are the spin-orbit splittings in excited and ground states respectively, and δE^e and δE^g are the strain splitting coefficients in the excited and ground states respectively. The correlation between ground and excited state splittings in Figure 3d gives the ratio $\delta E^e/\delta E^g = 1.688^{+0.008}_{-0.008}$ and it is the first time this has been determined for the SiV^- center. Only one study has reported uni-axial strain measurements on SiV^- centers in diamond [28].

Although the calibration of the strain is unknown in these NDs, the systematic observation of splittings enables a reliable identification of the intrinsic SiV^- spin-orbit splitting. Bayesian inference [29, 30] was used to find the most plausible λ_{SO}^e , λ_{SO}^g , $\delta E^e/\delta E^g$, and strain values for the SiV^- spectra. These results are illustrated in Figure 3e, and give zero-strain splittings of $46.3^{+2.5}_{-3.4}$ GHz and $252.0^{+1.3}_{-1.8}$ GHz for the ground and excited states respectively (the full posterior distributions are given in Supp. Mat.). These results also indicate that 13 of the 18 SiV^- spectra are in the “low transverse strain” situation, where the splittings are dominated by spin-orbit interaction (below about 40 transverse strain units). It is remarkable to find such a high proportion of low-strain SiV^- centres in small NDs.

Indistinguishability of photons from SiV^- in NDs

Resolving the fine-structure also provides the first opportunity to study the polarization behavior of single SiV^- center in NDs. In the absence of perturbations such as strain, the four optical transitions of the SiV^- ZPL are known to follow the polarization rules expected from group theory for spin-orbit split E states [25]. The taller “inside” lines B and C arise only from the dipole moment parallel to the SiV^- axis (Z), and have strong polarization contrast. The outer lines A and D arise from the perpendicular X, Y dipole moments, and viewing geometry means that these always appear “polarized perpendicular” to lines B and C (although A and D typically show less polarization contrast because they are not from a single dipole). Polarization dependence of the spectrum was recorded for many of the SiV^- sites found in NDs, and a typical example is shown in Figure 4a-d. As illustrated, the polarization behavior was the same as for SiV^- in low-strain bulk diamond. Similar behavior was observed for most of the 18 SiV^- spectra that resolved the four-line fine structure. This adds further support to the interpretation of minimal strain for these SiV^- centers in NDs, and also demonstrates access to experiments in a cross-polarized configuration. It was also noticed that the polarization properties and also ratios of the relative peak heights can change under the influence of different strain in the NDs.

As an indistinguishable photon source candidate, it is furthermore important to possess spectral stability within the range of lifetime-limited linewidth for sufficiently long time. A single scan of the resonant laser

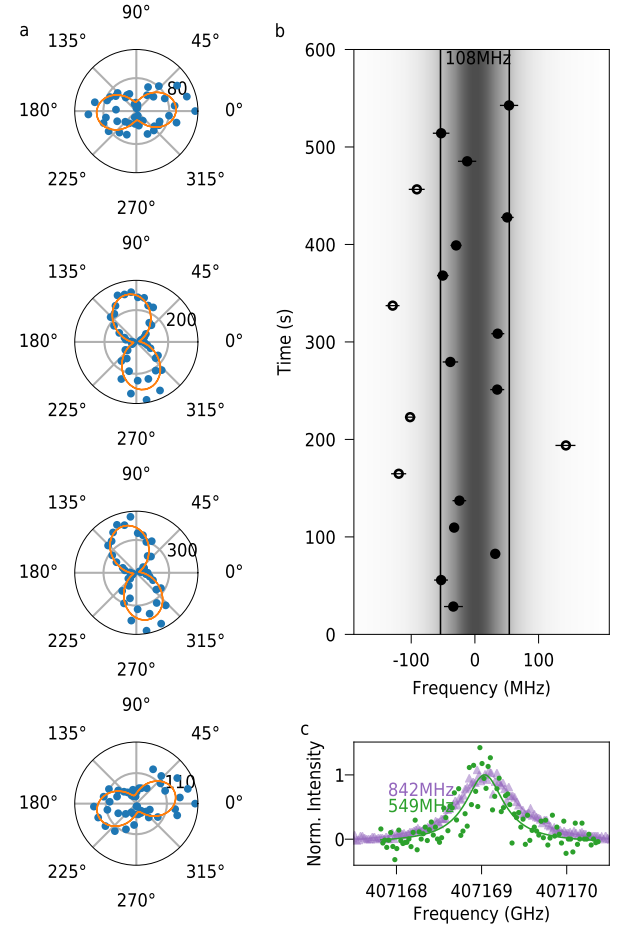


FIG. 4. Polarization of ZPL and spectral stability under resonance excitation of SiV^- in H-plasma treated NDs. **a** The polarization pattern of the 4-line fine structure assigned to corresponding optical transition, as shown in the lower spectrum. **b** Line position of a resonantly excited SiV^- center over 600 s. Occasionally blinking destroyed the symmetry of peaks, resulting in ill-fitted peak position (empty dots). Excluding such points, the frequency of such line stayed stably inside a range of 108 MHz, as indicated by the shadowed horizontal band. **c** With 600 nW of excitation power in front of the objective lens, an average linewidth (purple triangles) of 842 MHz as well as a minimum linewidth (green dots) of 549 MHz was measured from the same POI as in b. The peak heights were normalized to 1 for better comparison.

frequency across the resonance frequency of transition C with an excitation power of 600 nW leads to a narrowest linewidth of 549 MHz. 19 scans crossing the resonance frequency were recorded sequentially in 600 s. In five of these scans the SiV^- blinked off while the peak was scanned, leading to misfits of the peak position. The resonance frequencies of the remaining 14 scans were scattered in a frequency width of 108 MHz. The life time of excited state was extracted from $g^2(\tau)$ autocorrelation measurements, with the maximum value of 1.5 ns (See supplementary). This corresponds to a lifetime-limited

linewidth of 106 MHz, which is the same order as the observed variation in resonance frequency.

DISCUSSION

While it is significant that the H-plasma treatment has altered the spectral properties of SiV^- centers in these NDs, the mechanism for this change is less obvious. For NV^- centers it has been suggested that the strong band bending leads to holes being created in the valence band by H-plasma surface termination and absorption of H_2O [31]. Such discharge of the emitters close to the surface for plasma treated NDs containing SiV^- centers could lead to a reduction of the overall fluorescence as observed and, consequently, only emitters with larger distance to the diamond surface would remain active. These are likely to be the least strained SiV^- centers in the NDs, and so this explanation does account for the reduction in inhomogeneous ensemble linewidth and the high incidence of low-strain spectra. It is also possible that the more highly strained SiV^- centers are more susceptible to the discharging effect of the surface termination.

The reduction or elimination of spectral diffusion is significant, because part of the interest in SiV^- centers arose from the absence of spectral diffusion in low-strain bulk diamond [11]. Until now the desirable atom-like spectral properties were only reported for SiV^- centers in bulk diamond, although recently they were also seen for SiV^- centers in nanostructured diamond waveguides [32] leading to entanglement of two SiV^- centers [10]. The degradation of optical properties becomes in particular problematic for SiV^- centers in small NDs with diameter below 100 nm which are desired for hybrid approaches due to low light scattering and precise positioning capabilities. Spectral diffusion is a particular problem for the application in arrays of emitters, since inhomogeneity in spectral properties limits the optical coupling between nodes in the array. This has been a substantial problem for arrays of NV^- centers created through ion implantation and subsequent annealing and magnetic coupling has been demonstrated [33, 34].

While it is possible to prepare NDs containing both NV^- and SiV^- centers an alternative nano-manipulation protocol could as well be realized for NDs containing only SiV^- centers. Only the dipole alignment would require an alternative method. The high optical polarisation contrast shown in Figure 4a could be iteratively measured to achieve the desired rotational orientation without requiring NV^- centers and external magnetic fields. In the development of SiV^- arrays, such rotational manipulation is important to allow the alignment of optical dipoles for optimum coupling.

Since the position of NDs is determined from 2-D Gaussian fits, the uncertainties will increase with ND size. This can be partially solved by intermediate fitting steps, with the penalty of decreased speed of the manipulation process. At the end the most important

position accuracy is the location of the quantum emitter, which is then only limited by the size of the NDs. For improved super-resolution of the emitter position beyond the size of the ND other techniques, such as stimulated emission depletion microscopy could be utilized [35].

CONCLUSION

In this work we experimentally demonstrated how to recover symmetry-protected optical transitions of SiV^- centers in low-strained NDs. Together with manipulation capabilities of NDs on the nanometer-scale our work opens new routes for bottom-up assemblies of indistinguishable quantum emitter arrays and nanophotonic devices with deterministic coupling and emitter position control much better than diffraction limit. Individual NDs with size around 100 nm in diameter contain single SiV^- centers with bulk-like spectral stability. Such small NDs are most suitable for hybrid technology due to minimized light scattering and highest positioning precision. Furthermore, a diamond host with dimensions below 100 nm introduces a cut-off frequency in the phonon density-of-states beyond 50 GHz. The spin coherence time of SiV^- centers in bulk diamond is limited to ≈ 100 ns at 4 K due to interaction with acoustic phonons at a frequency corresponding to the ground state splitting of ≈ 50 GHz [26, 36–39]. Our work enables therefore new investigation of prolonged spin coherence times of SiV^- center in NDs at moderate temperatures. So far an extended spin coherence time T_2 of 13 ms and spin relaxation time T_1 exceeding 1 s in bulk were demonstrated at temperatures of 100 mK in dilution refrigerator [40].

METHODS

AFM positioning procedure

Prior to positioning, the ND region was imaged in the AFM and a reference ND was selected. The positions of other NDs were quickly estimated from a visual inspection of the topographic image, and a pushing distance was determined. The ND was moved using the AFM tip in contact mode, and the exact mechanics of this process depend on the shape of the AFM tip and the ND and the nature of their contact. It is possible for the ND to deviate sideways in undesired directions over the course of the movement, and it is important to avoid pushing the ND over the desired location. Positioning accuracy may be improved by iterating further cycles of position measurement and fine positioning, however this has not been performed here for two reasons. In the first place, the single-shot positioning accuracy is sufficient for many applications relying on optical coupling. Secondly, this single-shot procedure gives a useful lower bound on the nanomanipulation accuracy and is a valuable reference for further comparison.

After nanomanipulation, the ND positions were obtained with more precision by fitting each ND spot with a circular two-dimensional Gaussian function. The full-width at half-maximum was found to be about 75 nm, but the excellent height resolution of the AFM made it possible to locate the Gaussian fit within about 1 nm. Additional uncertainty arises from the fact that each ND may not be circularly symmetric (leading to an effective offset of

the Gaussian fit). However, these uncertainties are considered to be much smaller than the size of the ND, and so their contribution to the emitter position uncertainty is minimal.

The uncertainties in the calculated magnitude and angle of the magnetic field are a direct result of the 1 MHz uncertainty in the zero field splitting D . This error is less significant for changes in angles or magnetic fields than for the absolute values, as the D field values does not change for an NV in between measurements. The uncertainties of the angle and B-field were calculated using Gaussian error propagation with the package [41].

HPHT-Synthesizes of NDs

The Si doped NDs are synthesis following the receipe in reference [24]. High pressure high temperature synthesis of luminescent NDs was performed on the basis of fluoro-hydrocarbon growth system without catalyst metals [24]. Naphthalene $C_{10}H_8$ (Chemapol) and highly fluorinated graphite $CF_{1.1}$ (Aldrich Chemical) with the impurity content less than 0.5 % were used as initial hydrocarbon and fluorocarbon components of the growth system. Tetrakis(trimethylsilyl)silane $C_{12}H_{36}Si_5$ (Stream Chemicals Co.) was taken as the silicon doping compound. Ternary homogeneous mixture $C_{10}H_8$ - $CF_{1.1}$ - $C_{12}H_{36}Si_5$ with a Si/C atomic ratio of 0.07 were used as the initial material for diamond synthesis. The tablets (5 mm diameter and 4 mm height) of cold-pressing starting mixture were placed into graphite container which simultaneously served as a heater of the high pressure Toroid-type apparatus. The experimental procedure consisted of loading the high-pressure apparatus to 8 GPa at room temperature, then heating the sample to the desired temperature ($\sim 1200^\circ C$), followed by isothermal exposure of the sample during 20 s at this temperature. The obtained high-pressure states have been isolated by quenching to room temperature under pressure and then complete pressure release. The recovered diamond materials have been characterized under ambient conditions by using X-ray diffraction, Raman spectroscopy, scanning and transmission electron microscopies (SEM and TEM).

Size selection of NDs

After production the NDs were not size selected and ranged from nm size to a few micrometer size. In order to size select them centrifugation was employed. The NDs, which were in a solution of ethanol and micro water were dispersed in 1 ml of micro water which was then centrifuged at 2000 rpm and the liquid at the top was transferred to a new container. This process of dilution and centrifugation was repeated another 3 times for 1000 rpm, 500 rpm and 300 rpm. As the concentration was low after this process all new solutions were centrifuged at 5000 rpm and the liquid at the top mixed of each solution removed and stored in a separate container. The concentrated solution that was acquired with centrifugation at 2000 rpm carries the smallest NDs while the majority of which are around or smaller than 130 nm when observed by SEM on the same Ila diamond substrate as used in cryogenic measurements. Apart from the majority, the extremums of ND size, when observed by

SEM, were 30 nm and 280 nm. The resolving power of microscopy was constrained by the surface charging of non-electroconductive diamonds substrate, leading to poor image quality for NDs smaller than 30 nm. As for larger sized anomalies, over many SEM sessions only 3 NDs above 200 nm size were found.

Cryogenic confocal microscopy and Sample preparation

For lowest background fluorescence and best thermal conductivity, type-IIa diamond was chosen as substrate material (2×2 mm). Markers were etched on the surface with selective carbon milling by Helios 3D FEG. Substrates were cleaned in a boiling solution ($\approx 100^\circ C$) of $HC_1O_4:H_2SO_4:HNO_3$ (tri-acid mix). The untreated ND solution was diluted by chloroform and placed inside an ultra sonic bath for 10 min. 2 μ l of the diluted sample was spin coated onto the substrate at 5000 rpm for 40 seconds.

The sample was mounted on the cold-finger of a continuous flow helium cryostat, which was cooled to 8 K for imaging with a home-built confocal microscope. Experimental control was provided by the Qudi software suite [42]. The SiV^- centers were off resonantly excited by 532 nm green laser with $120 \pm 10 \mu W$ in front of the objective lens. Spectra were measured after a 560 nm long pass filter, and polarisation dependence was measured by rotating the fluorescence using a half-wave plate before recording spectra through a fixed Glan-Thompson polarizer. This prevents any polarisation dependence of the detection instruments from impacting the results. Statistical processing of spectra was performed using Bayesian inference (see Supp. Mat. for details), and Python packages emcee [43], Pymc and Pymc3 [44] were used to perform the Markov-chain Monte Carlo ensemble sampler computations.

H plasma treatment

The surface termination is carried out in a plasma assisted chemical vapour deposition (PACVD) reactor. The microwave cavity is formed by a glass cylinder in which the microwave antenna is placed and a movable sample plate, on which the NDs on a single crystal Ila type diamond are mounted. The chamber is pumped to a vacuum of 10^{-10} mbar before the process is started. Hydrogen at a flow rate of 300 sccm is pumped into the reactor whereby the pressure is increased stepwise to 25 mbar over 480 seconds. In the same time the MW power and temperature are increased, also stepwise, to 2.5 kW and $750^\circ C$, respectively. To stabilize the plasma, the resonator height is also adjusted and the microwave back reflection is set to a minimum, by optimizing the microwave conductor manually. These conditions are hold for 60 seconds before all parameters are stepwise decreased to zero in 390 seconds. During this whole time the NDs are exposed to the plasma which results in a hydrogen surface termination.

REFERENCES

-
- [1] S. Haroche, *Annalen der Physik* **525**, 753 (2013).
 - [2] D. J. Wineland, *Reviews of Modern Physics* **85**, 1103 (2013).
 - [3] C. Monroe and J. Kim, *Science* **339**, 1164 (2013).
 - [4] M. H. Devoret and R. J. Schoelkopf, *Science* **339**, 1169 (2013).
 - [5] M. Endres, H. Bernien, A. Keesling, H. Levine, E. R. Anschuetz, A. Krajenbrink, C. Senko, V. Vuletic, M. Greiner, and M. D. Lukin, *Science* **354**, 1024 (2016).
 - [6] J. L. O'Brien, A. Furusawa, and J. Vukovi, *Nature Photonics* **3**, 687 (2009).
 - [7] H. J. Kimble, *Nature* **453**, 1023 (2008).

- [8] S. Ritter, C. Nölleke, C. Hahn, A. Reiserer, A. Neuzner, M. Uphoff, M. Mücke, E. Figueroa, J. Bochmann, and G. Rempe, *Nature* **484**, 195 (2012).
- [9] T. Schröder, M. E. Trusheim, M. Walsh, L. Li, J. Zheng, M. Schukraft, A. Sipahigil, R. E. Evans, D. D. Sukachev, C. T. Nguyen, J. L. Pacheco, R. M. Camacho, E. S. Bielejec, M. D. Lukin, and D. Englund, *Nature Communications* **8**, 15376 (2017).
- [10] A. Sipahigil, R. E. Evans, D. D. Sukachev, M. J. Burek, J. Borregaard, M. K. Bhaskar, C. T. Nguyen, J. L. Pacheco, H. A. Atikian, C. Meuwly, R. M. Camacho, F. Jelezko, E. Bielejec, H. Park, M. Lonar, and M. D. Lukin, *Science* **354**, 847 (2016).
- [11] L. Rogers, K. Jahnke, T. Teraji, L. Marseglia, C. Müller, B. Naydenov, H. Schauffert, C. Kranz, J. Isoya, L. McGuinness, and F. Jelezko, *Nature Communications* **5**, 4739 (2014).
- [12] A. Sipahigil, K. Jahnke, L. Rogers, T. Teraji, J. Isoya, A. Zibrov, F. Jelezko, and M. Lukin, *Physical Review Letters* **113** (2014), 10.1103/PhysRevLett.113.113602.
- [13] C. Hepp, T. Müller, V. Waselowski, J. N. Becker, B. Pingault, H. Sternschulte, D. Steinmüller-Nethl, A. Gali, J. R. Maze, M. Atatüre, and C. Becher, *Physical Review Letters* **112** (2014), 10.1103/PhysRevLett.112.036405.
- [14] A. T. Collins, L. Allers, C. J. Wort, and G. A. Scarabrook, *Diamond and Related Materials* **3**, 932 (1994).
- [15] S. Tamura, G. Koike, A. Komatsubara, T. Teraji, S. Onoda, L. P. McGuinness, L. Rogers, B. Naydenov, E. Wu, L. Yan, F. Jelezko, T. Ohshima, J. Isoya, T. Shinada, and T. Tani, *Applied Physics Express* **7**, 115201 (2014).
- [16] J. Wolters, G. Kewes, A. W. Schell, N. Nüsse, M. Schöngeng, B. Löchel, T. Hanke, R. Bratschitsch, A. Leitenstorfer, T. Aichele, and O. Benson, *physica status solidi (b)* **249**, 918 (2012).
- [17] M. Y. Shalaginov, V. V. Vorobyov, J. Liu, M. Ferrera, A. V. Akimov, A. Lagutchev, A. N. Smolyaninov, V. V. Klimov, J. Irudayaraj, A. V. Kildishev, A. Boltasseva, and V. M. Shalae, *Laser & Photonics Reviews* **9**, 120 (2015).
- [18] A. Huck and U. L. Andersen, *Nanophotonics* **5** (2016), 10.1515/nanoph-2015-0153.
- [19] U. Jantzen, A. B. Kurz, D. S. Rudnicki, C. Schäfermeier, K. D. Jahnke, U. L. Andersen, V. A. Davydov, V. N. Agafonov, A. Kubanek, L. J. Rogers, and F. Jelezko, *New Journal of Physics* **18**, 073036 (2016).
- [20] A. Huck, S. Kumar, A. Shakoov, and U. L. Andersen, *Physical Review Letters* **106** (2011), 10.1103/PhysRevLett.106.096801.
- [21] G. Balasubramanian, I. Y. Chan, R. Kolesov, M. Al-Hmoud, J. Tisler, C. Shin, C. Kim, A. Wojcik, P. R. Hemmer, A. Krueger, T. Hanke, A. Leitenstorfer, R. Bratschitsch, F. Jelezko, and J. Wrachtrup, *Nature* **455**, 648 (2008).
- [22] V. M. Acosta, *Optical magnetometry with nitrogen-vacancy centers in diamond* (University of California, Berkeley, 2011).
- [23] E. Neu, C. Arend, E. Gross, F. Guldner, C. Hepp, D. Steinmetz, E. Zscherpel, S. Ghodbane, H. Sternschulte, D. Steinmüller-Nethl, Y. Liang, A. Krueger, and C. Becher, *Applied Physics Letters* **98**, 243107 (2011).
- [24] V. A. Davydov, A. V. Rakhmanina, S. G. Lyapun, I. D. Ilichev, K. N. Boldyrev, A. A. Shiryayev, and V. N. Agafonov, *JETP Letters* **99**, 585 (2014).
- [25] L. J. Rogers, K. D. Jahnke, M. W. Doherty, A. Dietrich, L. P. McGuinness, C. Müller, T. Teraji, H. Sumiya, J. Isoya, N. B. Manson, and F. Jelezko, *Physical Review B* **89** (2014), 10.1103/PhysRevB.89.235101.
- [26] K. D. Jahnke, A. Sipahigil, J. M. Binder, M. W. Doherty, M. Metsch, L. J. Rogers, N. B. Manson, M. D. Lukin, and F. Jelezko, *New Journal of Physics* **17**, 043011 (2015).
- [27] A. Dietrich, K. D. Jahnke, J. M. Binder, T. Teraji, J. Isoya, L. J. Rogers, and F. Jelezko, *New Journal of Physics* **16**, 113019 (2014).
- [28] H. Sternschulte, K. Thonke, R. Sauer, P. C. Münzinger, and P. Michler, *Physical Review B* **50**, 14554 (1994).
- [29] E. T. Jaynes, *Probability Theory: the Logic of Science* (Cambridge University Press, 2003).
- [30] P. Gregory, *Bayesian Logical Data Analysis for the Physical Sciences: A Comparative Approach with Mathematica Support* (Cambridge University Press, 2005).
- [31] M. V. Hauf, B. Grotz, B. Naydenov, M. Dankerl, S. Pezzagna, J. Meijer, F. Jelezko, J. Wrachtrup, M. Stutzmann, F. Reinhard, and J. A. Garrido, *Physical Review B* **83**, 081304 (2011).
- [32] R. E. Evans, A. Sipahigil, D. D. Sukachev, A. S. Zibrov, and M. D. Lukin, *Physical Review Applied* **5** (2016), 10.1103/PhysRevApplied.5.044010.
- [33] J. Meijer, B. Burchard, M. Domhan, C. Wittmann, T. Gaebel, I. Popa, F. Jelezko, and J. Wrachtrup, *Applied Physics Letters* **87**, 261909 (2005).
- [34] J. R. Rabeau, P. Reichart, G. Tamanyan, D. N. Jamieson, S. Praver, F. Jelezko, T. Gaebel, I. Popa, M. Domhan, and J. Wrachtrup, *Applied Physics Letters* **88**, 023113 (2006).
- [35] T. A. Klar and S. W. Hell, *Optics Letters* **24**, 954 (1999).
- [36] L. J. Rogers, K. D. Jahnke, M. H. Metsch, A. Sipahigil, J. M. Binder, T. Teraji, H. Sumiya, J. Isoya, M. D. Lukin, P. Hemmer, and F. Jelezko, *Physical Review Letters* **113** (2014), 10.1103/PhysRevLett.113.197601, arXiv: 1410.1355.
- [37] B. Pingault, J. N. Becker, C. H. Schulte, C. Arend, C. Hepp, T. Godde, A. I. Tartakovskii, M. Markham, C. Becher, and M. Atatüre, *Physical Review Letters* **113** (2014), 10.1103/PhysRevLett.113.263601.
- [38] J. N. Becker, J. Görlitz, C. Arend, M. Markham, and C. Becher, *Nature Communications* **7**, 13512 (2016).
- [39] B. Pingault, D.-D. Jarausch, C. Hepp, L. Klintberg, J. N. Becker, M. Markham, C. Becher, and M. Atatüre, *Nature Communications* **8**, 15579 (2017).
- [40] D. Sukachev, A. Sipahigil, C. Nguyen, M. Bhaskar, R. Evans, F. Jelezko, and M. Lukin, *Physical Review Letters* **119** (2017), 10.1103/PhysRevLett.119.223602.
- [41] E. O. LEBIGOT, “Uncertainties: a python package for calculations with uncertainties,”.
- [42] J. M. Binder, A. Stark, N. Tomek, J. Scheuer, F. Frank, K. D. Jahnke, C. Müller, S. Schmitt, M. H. Metsch, T. Uden, T. Gehring, A. Huck, U. L. Andersen, L. J. Rogers, and F. Jelezko, *SoftwareX* **6**, 85 (2017).
- [43] D. Foreman-Mackey, D. W. Hogg, D. Lang, and J. Goodman, *Publications of the Astronomical Society of the Pacific* **125**, 306 (2013).
- [44] A. Patil, D. Huard, and C. J. Fonnesbeck, *Journal of Statistical Software* **35**, 1 (2010).

ACKNOWLEDGEMENTS

We acknowledge G. Neusser and the FIB Center UUlM for etching the markers into the diamond IIA substrate. We acknowledge help from F. Frank (Uni Ulm) with the AFM, and A. Gilchrist (Macquarie Uni) for guiding discussions in developing the Bayesian analysis. LR is the recipient of an Australian Research Council Discovery Early Career Award (project number DE170101371) funded by the Australian Government. VAD thanks the Russian Foundation for Basic Research (Grant No. 18-03-00936) for financial support. YL is currently supported by Sino-German (CSC-DAAD) Postdoc Scholarship Program (57251553). ABF acknowledges support of the Carl-Zeiss Foundation. FJ acknowledges support of the DFG, BMBF, VW Stiftung and EU (ERC, DIADEMS). AK acknowledges the generous support of the DFG, the Carl-Zeiss Foundation, IQST, the Wissenschaftler-Rückkehrprogramm GSO/GZS.

AUTHOR CONTRIBUTIONS

Experiments were conceived by LR, AK, and FJ. OW, ABF, and LR performed the spectroscopic measurements; OW and CO performed the surface treatment; YL and LA performed nanomanipulation of the nanodiamonds. ABF and OW did the sample preparation. ABF performed the SEM measurements. LR and OW performed the Bayesian strain analysis. VAD and VA synthesized the NDs with SiV- centers. The manuscript was written by OW, ABF, LR, and AK and all authors discussed the results and commented on the manuscript.

COMPETING FINANCIAL INTERESTS

The authors declare no competing financial interests.